New Insights into the Mechanism of TiO 2 Photocatalysis: Thermal Processes beyond the Electron − Hole Creation

ARTICLE *in* THE JOURNAL OF PHYSICAL CHEMISTRY C · OCTOBER 2011

Impact Factor: 4.77 · DOI: 10.1021/jp112243q

4 AUTHORS, INCLUDING:

Cecilia Beatriz Mendive
Universidad Nacional de Mar del Plata
21 PUBLICATIONS **632** CITATIONS
SEE PROFILE

David Hansmann
Universidad Nacional de Mar del Plata
8 PUBLICATIONS **25** CITATIONS
SEE PROFILE

THE JOURNAL OF PHYSICAL CHEMISTRY C

ARTICLE

pubs.acs.org/JPCC

New Insights into the Mechanism of TiO_2 Photocatalysis: Thermal Processes beyond the Electron−Hole Creation

Cecilia B. Mendive,*[,†,‡] David Hansmann,[§] Thomas Bredow,[§] and Detlef Bahnemann[‡]

[†]Departamento de Química, Facultad de Ciencias Exactas y Naturales, Universidad Nacional de Mar del Plata, Dean Funes 3350, 7600 Mar del Plata, Argentina

[‡]Institut fuer Technische Chemie, Leibniz Universitaet Hannover, Callinstr. 3, D-30167 Hannover, Germany

[§]Institute for Physical and Theoretical Chemistry, Universitaet Bonn, Wegelerstr. 12, D-53115 Bonn, Germany

ABSTRACT: Infrared spectroscopic studies of a UVA irradiated layer of TiO_2 nanoparticles in contact with an aqueous solution free of any photocatalytic degradable compound showed that a volume of water is incorporated in the layer. Such a phenomenon is attributed to a mechanism of deaggregation of particles agglomerates resulting from the capacity of the system to use the energy released by recombination of photogenerated electrons and holes. In this mechanism, bonds responsible for maintaining nanoparticles agglomerated are broken, allowing the particles to separate. Water molecules fill the space in between the particles, and it is experimentally evinced by the increase in the band corresponding to the bending mode of water. Under UVA illumination, the TiO_2 exposed area thus increases, hence promoting an enhancement of the adsorption capacity of the photocatalyst.

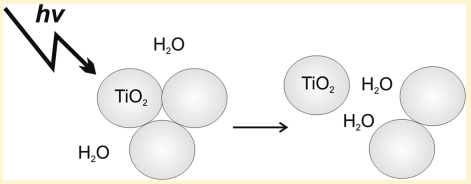

INTRODUCTION

Initiated by the findings of Honda and Fujishima in 1972,[1] who used TiO_2 for the photoassisted electrochemical splitting of water, considerable efforts have been invested in studying TiO_2 and its related photoinduced reactions. Numerous reviews concerning photocatalytic and photoelectrochemical reactions, focusing on materials, reactor setups, or mechanistic aspects,[2−10] have been published. In addition, other uses of photocatalysis, such as photocatalytic organic synthesis,[11−14] can be regarded as emerging topics. Interesting reviews on all types of materials employed for semiconductor photocatalysis can thus be found describing in depth the different developed approaches.[15−19] The development of new materials for photocatalytic applications exhibiting high efficiencies or being able to utilize also visible light for the initiation of the photocatalytic process is currently the target of many research projects in this field.

There is, however, still a considerable deficit concerning the basic processes that constitute the overall photocatalytic transformation. Although the detailed mechanism of photocatalysis varies with different pollutants, it is commonly agreed that the primary reactions responsible for the photocatalytic effect are interfacial redox reactions of electrons and holes that are generated when the semiconductor catalyst is exposed to light of sufficient energy (cf. figure 1 of ref 2)

As illustrated in Figure 1, the mechanism of redox processes induced by light absorption in a photocatalytic system is usually presented in diagrams showing one single semiconductor nanoparticle in which the absorption of a photon with an energy exceeding its bandgap energy generates an electron/hole pair (process 1) that either recombines (process 2) or induces two redox processes (processes 3 and 4), both of which take place in close vicinity on the particle's surface. However, during the past decade, we have collected considerable evidence that this mechanistic picture is oversimplified.[20−22] As illustrated in Figure 2, metal oxide nanoparticles tend to form 3D networks via a self-aggregation mechanism.[20] HRTEM analysis of these aggregates showed that herein the particle−particle contacts do not form in an arbitrary manner but rather involve the exact alignment of the atomic planes of all involved particles. Consequently, the resulting aggregates can be regarded as arrays of nanowires that should allow the transfer of charge carriers without much interference of interfacial trap processes (cf. Figure 2, right).

This so-called "antenna effect" has meanwhile been observed by various research groups (i.e., list of references given in ref 21) and should in fact be regarded as a new basic concept for photocatalytic systems. Excitons formed through the absorption of light in one of the nanoparticles within this particle framework are likely to be transported throughout until arriving at a suitable trap site. The latter can, for example, be formed through the adsorption of electron acceptors, donors, or both on one of the particles belonging to the aggregate. Once one of the charge carriers has been trapped, that is, has been involved in a redox reaction with the adsorbate, the other charge carrier can continue its "journey" through the particle network until reacting itself.[20] Obviously, the particle network replaces the individual photocatalyst particle shown in Figure 1, thus resulting in an improved photocatalytic activity of the overall system, that is, through a cooperative effect within the network. The good electron mobility within 3D TiO_2 agglomerates actually presents one basic

Received: December 23, 2010
Revised: September 4, 2011
Published: September 05, 2011

functionality of dye-sensitized solar cells and has thus been thoroughly investigated.

We are therefore convinced that it is of utmost importance to gain further knowledge at the fundamental level concerning the underlying mechanisms taking place on classical photocatalytic materials, such as TiO_2, to advance technological approaches and to improve applications. In particular, the interaction of UV(A) light with TiO_2 still poses multiple challenging questions, most of which so far have not been answered univocally. Fundamental investigations focusing on the interaction of light with single photocatalyst nanoparticles and with their ensembles are hence required.

Several mechanisms operating in TiO_2 have been discussed in the last years. They contemplate different viewpoints, ranging from those based on atomic scale considerations[23,24] to extrinsic properties of the materials[25,26] and also involving the collective action of nanoparticles aggregates.[22,27] Most commonly, experimental studies concerning, for example, new (and better?) photocatalysts that are being synthesized will focus on the "heart" of photocatalysis, that is, on the creation of chemically active electron−hole (e−h+) pairs. Their respective reactions with selected probe molecules will be followed to obtain (hopefully) useful knowledge of the active part of the process and thus to describe the entire photocatalytic reaction. However, in most cases the photonic efficiency values of the underlying electron transfer processes do not exceed 1%; that is, 99% of all available photons are not utilized by the process. Consequently, the fate of the remaining photons not leading to any photocatalytic conversion (oxidative and reductive reactions) is not considered! One may suggest that the energy that these photons have deposited within the exited photocatalyst particle is easily lost by recombination and subsequent dissipation as heat. Alternative mechanisms somehow utilizing this energy and thus contributing considerably to the overall photocatalytic reaction cannot a priori be ruled out.

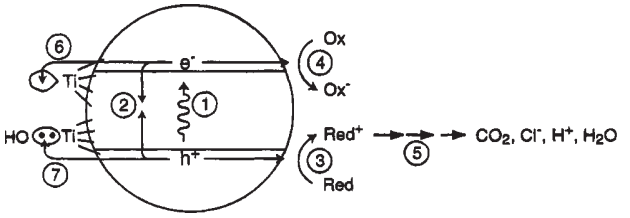

Figure 1. Primary steps in the mechanism of photocatalysis: (1) formation of charge carriers by photon absorption, (2) charge carrier recombination, (3) initiation of an oxidative pathway by a valence-band hole, (4) initiation of a reductive pathway by a conduction-band electron, (5) further thermal (e.g., hydrolysis or reactions with active oxygen species) and photocatalytic reactions to yield mineralization products, (6) trapping of a conduction-band electron at a Ti(IV) site to yield Ti(III), and (7) trapping of a valence-band hole at a surface titanol group.

Therefore, the emphasis of the work described in this Article has been laid on the further understanding of the role of thermal processes within the overall framework of photocatalysis. As Pagel et al.[22,27] have already anticipated, thermal processes beyond the redox reactions performed by the photogenerated e−h+ pairs that managed to survive recombination, can, most certainly, yield non-negligible effects. Furthermore, considering their relative magnitude, it is obvious that the (mostly neglected) thermal effects should potentially have a considerable impact on the entire photocatalytic process. Hence, a more complete mechanistic picture concerning the interaction of TiO_2 with excitation light for the production of e−h+ pairs should include considerations concerning thermal processes arising from recombined and thus chemically inactive e−h+ pairs. For the present study, we have chosen to explore the effects of UV(A) irradiation on a compact particulate system. Employing infrared spectroscopy as the monitoring means, UV(A) irradiated layers of TiO_2 nanoparticles have been investigated in contact with pure water. Aqueous solutions free of any compound able to undergo a photocatalytic conversion have been selected to focus clearly on the phenomena involving the photocatalyst particles, that is, avoiding contributions and possible interferences from the photocatalytic reactions and their products. Spectral features observed upon UV(A) illumination reveal structural changes of the system that are discussed in the frame of the existing mechanisms for photoinduced processes and for TiO_2 photocatalysis.

EXPERIMENTAL PROCEDURES

Pure anatase nanoparticles, the commercial product S230 from Kemira with 230 $m^2 \cdot g^{-1}$ (single-point BET adsorption measurements) and particle size of 4−7 nm was employed. Detailed information about this TiO_2 material can be found elsewhere.[28] Other reagents used in this work were of analytical grade and

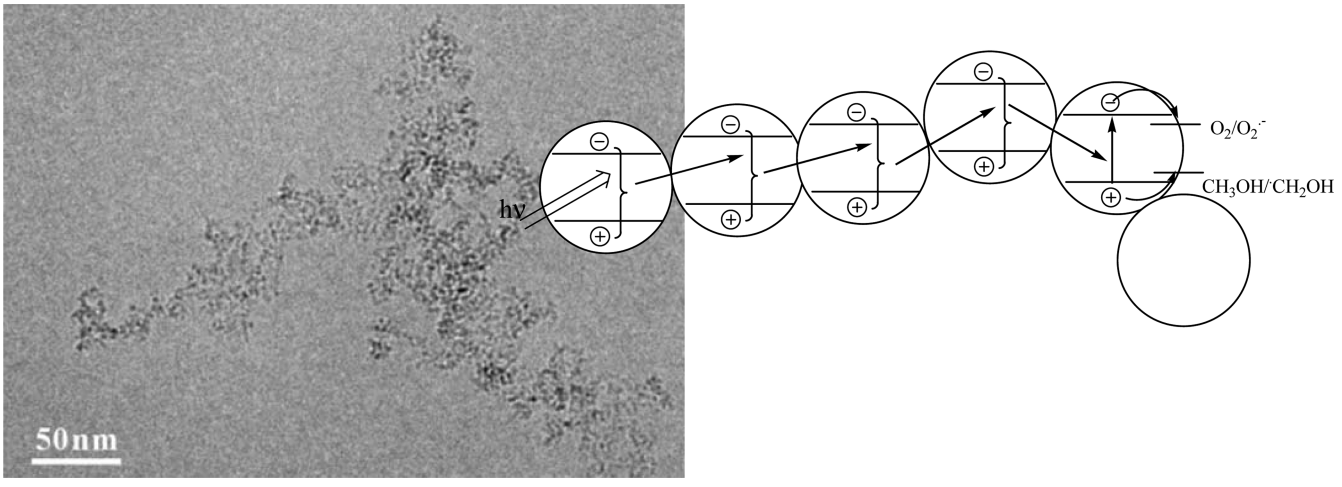

Figure 2. Cryo-TEM image of 0.5 at % Fe(III)-doped TiO_2 nanoparticles (left) and scheme explaining the increased photocatalytic activity through energy/exciton transfer in aggregated photocatalyst particles, that is, the antenna effect (right) (ref 20).

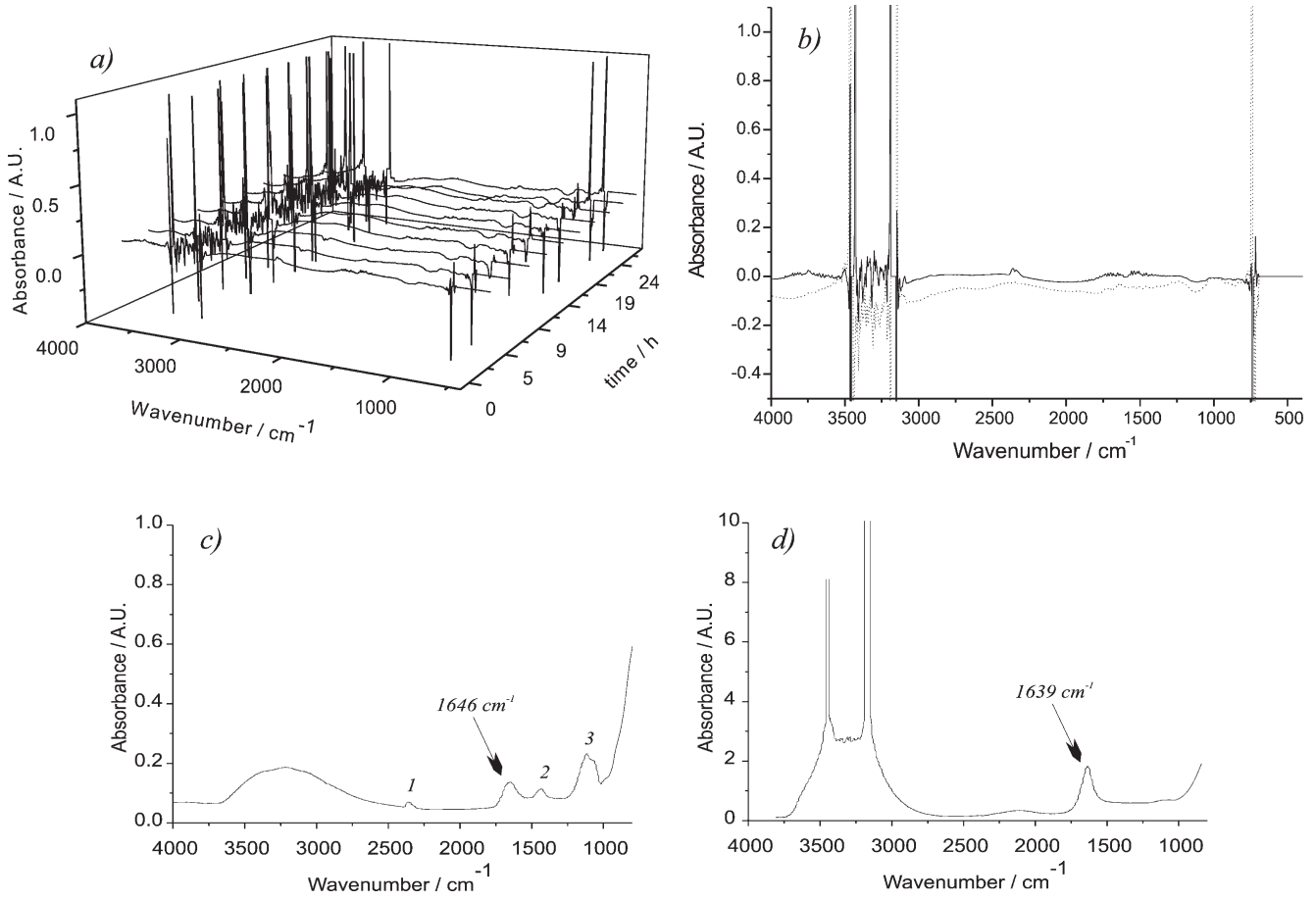

Figure 3. (a) Evolution in time of the ATR-FTIR spectra of the TiO_2 layer in contact with the aqueous solution in the dark for 25 h, (b) the first (dotted line) and last spectra (solid line), (c) ATR-FTIR spectrum of the dry TiO_2 layer, and (d) upon contact with the aqueous solution. The first spectrum d was used as reference in panels a and b. The naked ZnSe crystal was used as reference in panel c. The bending mode of water was marked with an arrow on spectra c and d, showing a slight shift of the band corresponding to the adsorbed and bulk status of the water molecules. The bands marked with numbers are assigned to (1) incomplete cancellation of CO_2 present in the interferometer and (2) and (3) traces of organic impurities insoluble in water and Se^{2-} oxidation products during the TiO_2 layer deposition, respectively, that remain unchanged along the entire experiment.

used as received. Deionized water from a Sartorius Arium 611 apparatus (conductivity = 0.182 μS m^{-1}) was always employed for the preparations of the solutions and suspensions.

The ATR-FTIR spectra were recorded on a BOMEM MB 122 instrument that was equipped with a liquid-N_2-cooled MTC-A detector and a Pike Technologies horizontal ATR unit with a ZnSe crystal of 45° and nine reflections in the upper face.

The UVA illumination source was supplied by two tubes (PHILIPS CLEO 15W), with a maximum emission at wavelengths between 300 and 400 nm placed directly above the ATR unit. The distance to the lamp was adjusted to provide 0.6 mW·cm^{-2}. Details of the setup construction can be found in ref 29.

A TiO_2 layer was deposited on the ZnSe ATR crystal (2.3 g·m^{-2} and 1−3 μm thick)[28,29] by drying at room temperature an aliquot of 200 μL of a 5.75 g·L^{-1} TiO_2 suspension together with 200 μL of water. (See refs 28 and 29.) Prior to the production of the TiO_2 thin layer, the ATR prism surface was cleaned by polishing with 1 μm diamond paste (Metadi II, polishing grade) and rinsed with methanol and deionized water. Therefore, identical initial conditions for every experiment were always restored. Sequential spectra of the TiO_2 layer equilibrated with the circulating aqueous solution were collected in the dark and under UVA illumination. Each final spectrum was the average of 250 scans and has a spectral resolution of 4 cm^{-1}.

For all experiments, 30 mL of circulating 0.01 M KNO_3 organic compounds-free solution was employed at a flow rate of ∼4 mL·min^{-1}. Eventual organic impurities present in the solutions were not detected by any analytical instrumentation. The pH of the circulating solution was fixed and kept constant at 3.70 ± 0.02 with a programmed dosing unit. During the entire experiment the solution was constantly purged with O_2.

To obtain a specimen for transmission electron microscopy (TEM) specimen, a 10 μL drop of powder suspension was applied from a pipet to a 300-mesh copper-supported continuous carbon foil (Quantifoil) and dried under an infrared lamp. TEM was performed at 200 kV on a field-emission instrument of the type JEOL JEM-2100F with an ultra-high-resolution pole piece that provides a point-resolution better than 0.19 nm. Micrographs were obtained in bright-field (BF) and phase contrast.

■ RESULTS AND DISCUSSION

A TiO_2 layer in contact with an aqueous organic compounds-free solution was monitored for 25 h in the dark (Figure 3) and under 7.9 h of UVA irradiation (Figure 4). The noisy features in the 3500 to 3000 cm^{-1} spectral window of Figure 3a,b, and Figure 4, corresponding to the stretching mode of water liquid water, result

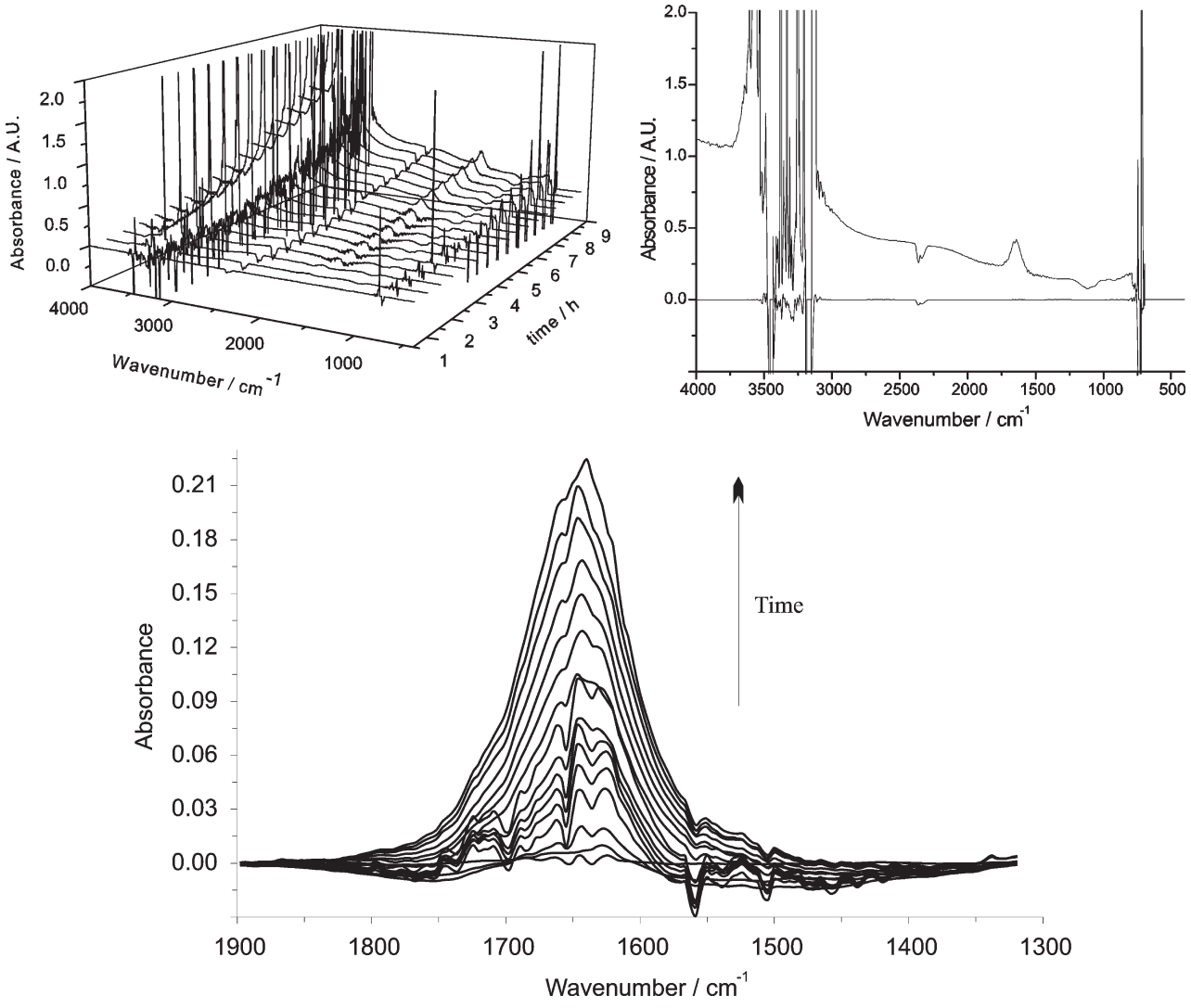

Figure 4. Evolution in time of the ATR-FTIR spectra of the same TiO_2 layer as in Figure 3 but under 7.9 h of UVA illumination. (The first spectrum was used as reference.) A baseline correction was applied to the spectral window between 1300 and 1900 cm^{-1}.

from incomplete cancellation of very intense absorptions. (The first spectrum was used as reference.) A similar situation occurs in the region under 1000 cm^{-1}, where the TiO_2 is not transparent to IR. Although water also absorbs around 1643 cm^{-1} (bending δ_{HOH} band), no such a features are observed in this region upon subtraction of the reference but instead the development and increase in a band of water upon continuous irradiation of the system (Figure 4). Figure 3c shows the spectrum of the dry TiO_2 layer in which much less intense water absorption bands, due to surface water present in the system, can be clearly depicted. Incomplete cancellations of gaseous CO_2 (bands at 2360 and 2343 cm^{-1}) and water vapor (fine spectral bands above 3560 cm^{-1} and in the region between 2000 and 1320 cm^{-1}) are also observed in Figure 3b.

The evolution in time of the ATR-FTIR spectra in Figure 3 shows no significant spectral changes for the TiO_2 layer under dark conditions. Furthermore, it demonstrates that the TiO_2 layer thus prepared in contact with the continuously circulating solution appears to be stable after 25 h.

Spectral changes upon UVA irradiation of the system (Figure 4) can be observed almost immediately, for example, within the first 30 min. Interestingly, the background lifts up and in a more pronounced manner at higher wavenumbers. The background lifting can be interpreted as a very broad band starting at ~1000 cm^{-1} extending beyond 4000 cm^{-1}. This latter feature was also observed by other researchers, and it has been attributed to the photoexcitation of electrons into a continuum of states within the conduction band.[30,31] In the present work, we will focus on the interpretation of the developed bending mode of water, which, interestingly, does not arise from instabilities of the layer but occurs only under UVA irradiation of the system.

Figure 4 clearly shows that there is an increase in the bending mode of water. Whether these water molecules are adsorbed is impossible to deduce from the spectra, and in the case of adsorbed water, according to molecular dynamics investigations of water adsorption on rutile,[32] the bending modes of nondissociated and a dissociated (OH group) molecules are manifested as bands rising at 1640 and 1625 cm^{-1}, respectively. It is worthy to note that as the exact frequency for water adsorption may slightly differ when taking into account different crystallographic faces of TiO_2,[33] especially comparing the case of anatase and rutile,[29] the band observed around 1640 cm^{-1} is therefore interpreted as an average of all frequencies corresponding to water adsorption on

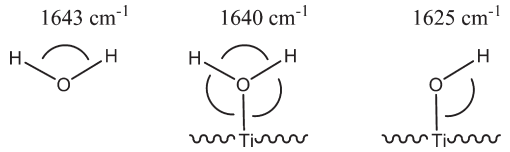

Figure 5. Bending modes of adsorbed water and OH groups.

the many nanocrystals (nanoparticles) constituting the TiO_2 layer here employed, which expose a range of different crystallographic faces.[34] In summary, three different possibilities can give rise to the bending mode observed in the spectra: not adsorbed, adsorbed nondissociated, and adsorbed dissociated water molecules. (See Figure 5.)

Several and ingenious mechanisms regarding the interaction of UVA light and TiO_2 have been suggested by different research groups. Fujishima, Hashimoto, and coworkers[23] have used the idea of photogenerated surface OH groups to explain the photoinduced hydrophilicity acquired by TiO_2 surfaces, specifically that of the rutile (110) face. In that approach, new surface OH groups arise from the combined effect of the cleavage of some Ti−O bonds at the surface and the subsequent dissociative chemisorption of water. Yates and coworkers[25] forwarded the hypothesis that the photocatalytic removal of adsorbed hydrocarbon impurities enables water droplets to spread out. Finally, Anpo and coworkers[24] suggested that the TiO_2 surface is covered by clusters of adsorbed water where a particular hydrogen bonds distribution is responsible to maintain a certain droplet shape. Upon evaporation of some water molecules from those clusters by the use of the residual heat from the illumination source, the hydrogen bond distribution is altered, leading to a change in the shape of the clusters; in particular, the clusters flatten and the hydrophilicity of the material is evinced. Additionally, the researchers suggest the coexistence of adsorbed hydrocarbon impurities that are removed by photocatalysis contributing to the observed photoinduced hydrophilic effect on TiO_2. In that sense, Anpo's and Yates's suggestions meet a common point.

Because the TiO_2 surface is in contact with liquid water, the consideration of the water clusters suggested by Anpo does not apply. However, the removal of hydrocarbon impurities suggested by both Anpo and Yates can be considered. Unlikely, this extension to explain enhanced water adsorption is less straightforward because the increase in spectral area is large. Upon impurities removal, additional water molecules would also be in a position to access fresh surface and contribute to the observed spectral changes. It should be noted that the postulated release of impurities is not seen by changes in the spectra in the 2900 to 2800 cm^{-1} region where ν_{CH} frequencies[35] locate. Furthermore, the accessibility of fresh water molecules to the portion of TiO_2 surface previously occupied by adsorbed impurities will definitively lead to chemisorption of water. In that case, it will likely occur dissociatively,[29,36,37] albeit associative chemisorption cannot be completely ruled out. Because of the newly adsorbed water entering the optical pathway of the probed system, a small increase in the bending mode should be observed. In a similar manner, if only the mechanism suggested by Fujishima and Hashimoto takes place, then the bending modes corresponding to the photogenerated surface OH groups should give rise to the band in Figure 4. Basically, by means of this mechanism, there should be an increase in the intensity of the band assigned to the stretching mode, that is, the region between 4000 and 3000 cm^{-1}. This spectral region is wide, and because of the present experimental conditions, such an increase is not possible to be observed. Because the optical path of the IR evanescent wave is larger than the thickness of a single monolayer of adsorbed water, those molecules that are not adsorbed must be strictly considered, and the assignment of the bending mode band to the solely adsorbed OH groups is unrealistic.

In the past, we observed a considerably enhancement of the aqueous oxalic acid adsorption capacity of TiO_2 surfaces under UVA irradiation.[26] Such a puzzling effect led us to the suggestion of a mechanism involving the creation of new adsorption sites by means of a photothermal-desorption of coadsorbed water molecules. The idea originated on the basis of the thermal energy released in the recombination process of the photogenerated electron−hole pairs. We postulated that this nonradiative and localized freed energy might be used by the system to desorb water molecules. Although some experimental evidence supporting this hypothesis has been provided by other researchers, in which water molecules are desorbed from the TiO_2 surface under UVA illumination[38] and UV-induced local heating effects were observed in TiO_2 nanocrystals,[39] a sounded proof is still missing. (This model would just account for a dynamic exchange of chemisorbed water without any change in the bending mode band.) Although this model is out of consideration for the explanation of the spectral feature of Figure 4, the remark falls on the importance of thermal processes in photocatalytic systems. Recently Pagel et al.[22,27] suggested an interested approach to study suspensions of nanoparticles, concluding that the total TiO_2 exposed surface increases under UVA illumination because of deaggregation of particles agglomerates. The mechanism counts on the light energy absorbed by the system that is partially used to separate particles chemically or physically adhered. The energy requirements are met, and newly exposed surface is therefore offered to the bulk solution for further adsorption. A point of remark is that this mechanism implies a new distribution of the particles: what was before an agglomerate is afterward a well-dispersed volume of suspended and isolated particles. Translating this situation to the TiO_2 layer of the present system, deaggregation upon UVA irradiation would mean a decrease in the particles density evinced along the normal direction because the layer could not elongate horizontally. In other words, the thickness of the TiO_2 layer would increase at the expense of a growing distance between the particles (Figure 6). Water would therefore fill the space, also adsorbing at the newly exposed surface but more importantly providing the corresponding resonator moieties for the increase in the bending mode frequency registered in Figure 4. It must be noted that in Figure 4 an accompanied decrease around 1100 cm^{-1} due to TiO_2 is also depicted while the band corresponding to the bending mode of water increases, but because of the close vicinity of noisy features, a consequence of subtracting high absorbances in that region, this observation should be taken with care.

The arrangement of the TiO_2 particles in the thin layer can also be compared with the agglomeration status in Pagel's suspensions. However, in our case, we assume that the deaggregation of agglomerates is a macroscopic mechanism similar to the dissolution of solids, in which the most outer particles preferentially separate first from the agglomerate instead of proceeding as a concerted mechanism in which all particles separate from each other at the same time to form a perfect suspension of monodispersed nanoparticles.

In dealing with quantitative aspects of the ATR technique, Harrick[40] merits a sounded contribution. We will briefly review his derivation and show the mathematical treatment we are able to employ in the frame of the suggested model (Figure 6) to draw

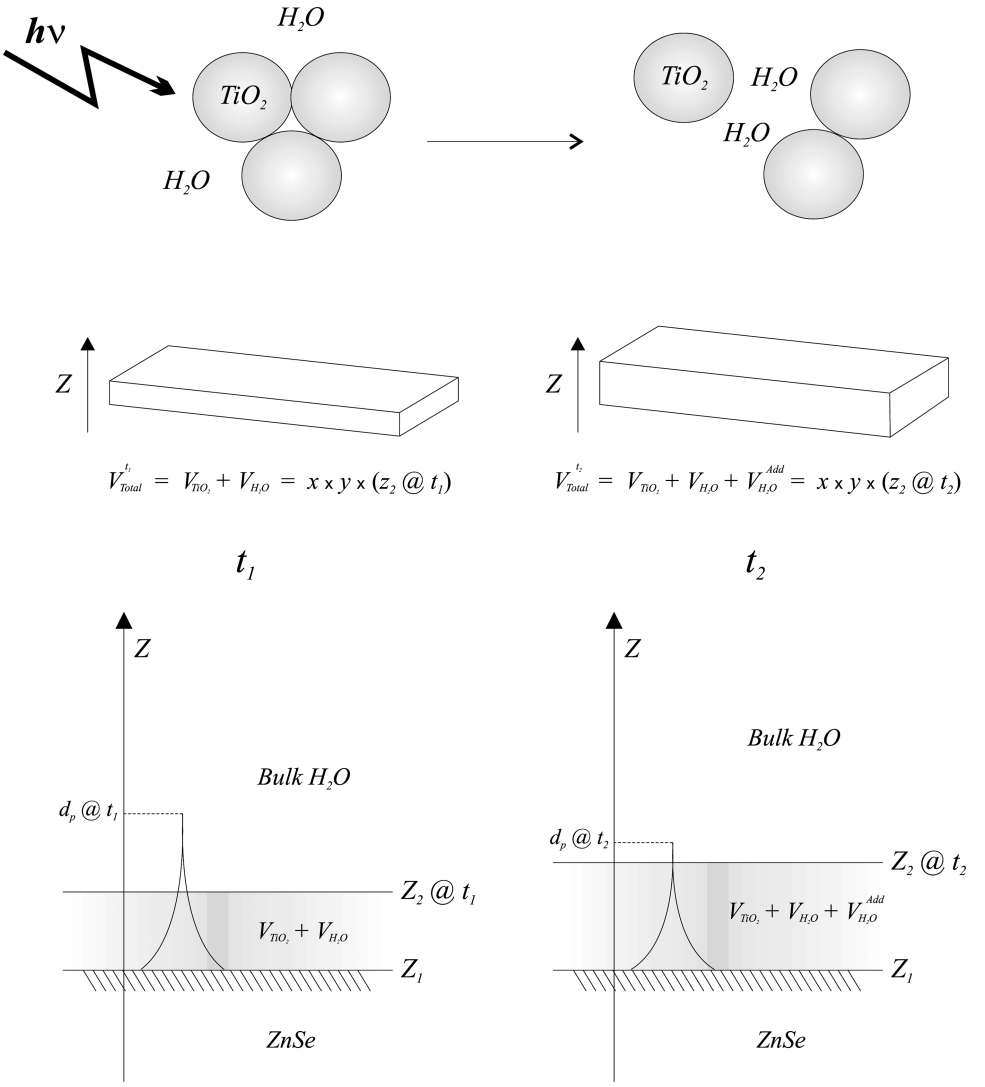

Figure 6. Suggested model and description of the TiO_2 layer thickness expansion in the z direction upon UVA irradiation at different times, t_1 and t_2. The variation of the penetration depth, d_p, is also indicated.

quantitative conclusions out of the observed spectral changes in Figure 4.

Upon one event of total internal reflection at the surface of the ZnSe crystal, the decrease in intensity of the escaping wave into the less dense medium is due to two reasons because it is an evanescent wave and because it is being absorbed (Figure 7).

In the simple case when the amount of absorbed light is small, the amplitude drops according to

$$E = E_0 e^{-z/d_p}$$

where the parameter d_p defines the penetration depth (Figure 6)

$$d_p = \frac{\lambda_1}{2\pi\sqrt{\sin^2\theta - \left(\frac{n_2}{n_1}\right)^2}}$$

with

$$\lambda_1 = \frac{\lambda_{vacuum}}{n_1}$$

to which E has decreased to $1/e$ of its value at the surface, E_0. E_0, in general, is not equal to the amplitude of the incoming wave (Figure 7). θ is the angle of incidence, and n_2 and n_1 are the refractive indexes of the less and the more dense media, respectively.

The intensity is therefore

$$I = E^2 = {E_0}^2 e^{-2z/d_p}$$

and if we assume that the amount of absorbed light is still proportional to the intensity at the place of absorption

$$dI = \alpha \cdot I \cdot dz$$

then we are able to obtain the amount of intensity absorbed.

The reflectivity, or reflecting power, for one reflection is simply defined as the ratio of the incoming, I_{in}, and leaving, I_{out}, intensities (Figure 7). Because the less dense medium absorbs, the absorption parameter a can be introduced as follows

$$R = \frac{I_{out}}{I_{in}} = 1 - a$$

dx.doi.org/10.1021/jp112243q |J. Phys. Chem. C 2011, 115, 19676–19685

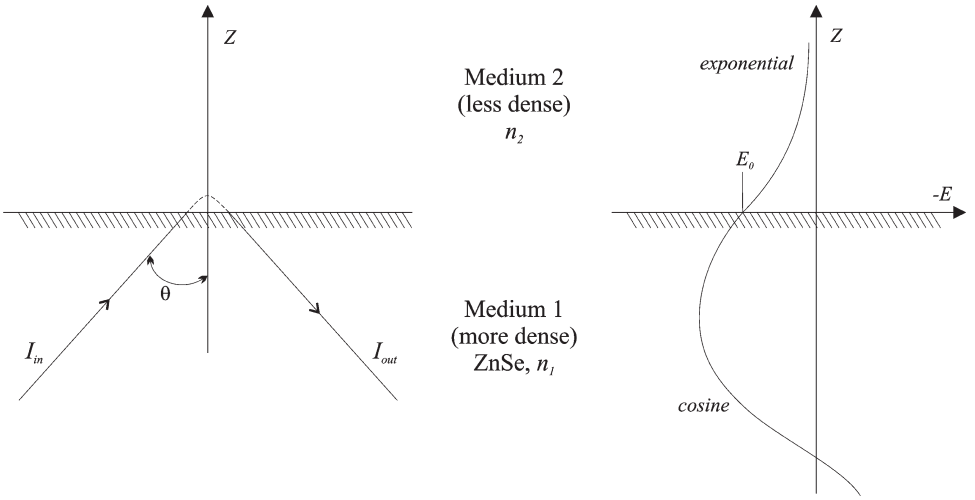

Figure 7. Schematic representation of the total internal reflection (left) and the standing wave amplitude pattern established at the interface (right).

Hence, the absorption parameter a is the total amount of absorbed light for a single reflection and can be determined experimentally via the measured absorbance, A (see below). The absorption parameter keeps close relation to the concentration of the absorbing species and can be derived integrating the amount of absorbed light, da, in an incremental volume of unit area and thickness, dz[41]

$$\mathrm{d}a = \frac{1}{\cos\theta}\cdot\alpha'\cdot E^2\cdot \mathrm{d}z$$

α' is the coefficient of extinction and has been described by Harrick as

$$\alpha' = \alpha\cdot\frac{n_2}{n_1}$$

where α is the coefficient of extinction that would be obtained in a transmission experiment.

The integration between two distances z_1 and z_2

$$a = \frac{n_2}{n_1}\cdot\frac{{E_0}^2}{\cos\theta}\int_{z_1}^{z_2}\alpha\cdot \mathrm{e}^{-2z/d_\mathrm{p}}\,\mathrm{d}z$$

assuming an homogeneous distribution of the absorbing species in z

$$\alpha \neq \alpha(z)$$

results

$$a = \alpha\cdot\frac{n_2}{n_1}\cdot\frac{1}{\cos\theta}\cdot\frac{\left(E^\mathrm{r}_{0,2\mathrm{II}}\right)^2 + \left(E^\mathrm{r}_{0,2\perp}\right)^2}{2}\cdot\frac{d_\mathrm{p}}{2}\left(\mathrm{e}^{-2z_1/d_\mathrm{p}} - \mathrm{e}^{-2z_2/d_\mathrm{p}}\right) \quad (1)$$

Transmission experiments rely on

$$\frac{I}{I_0} = \mathrm{e}^{-\alpha\cdot d}$$

where d is the optical path or the thickness of the material that light goes through. Because in our case $\alpha\cdot d$ is small, the transmittance can be approximated to

$$\frac{I}{I_0}\approx 1-\alpha\cdot d \quad (2)$$

which closely resembles the expression for the reflectivity

$$R = 1 - a$$

Hence

$$a = \alpha\cdot d \quad (3)$$

and d corresponds to the effective thickness, d_e, that is the thickness which would absorb the same amount of light in a transmission experiment

$$d = d_\mathrm{e} = \frac{n_2}{n_1}\cdot\frac{1}{\cos\theta}\cdot\frac{\left(E^\mathrm{r}_{0,2\mathrm{II}}\right)^2 + \left(E^\mathrm{r}_{0,2\perp}\right)^2}{2}\cdot\frac{d_\mathrm{p}}{2}\left(\mathrm{e}^{-2z_1/d_\mathrm{p}} - \mathrm{e}^{-2z_2/d_\mathrm{p}}\right) \quad (4)$$

with

$$E^\mathrm{r}_{0,2\mathrm{II}} = \frac{E^\mathrm{r}_{0,2\mathrm{II}}}{E_{1\mathrm{II}}} = \frac{2\cdot\cos\theta}{\sqrt{1-\left(\frac{n_2}{n_1}\right)^2}}\cdot\frac{\sqrt{2\cdot\sin^2\theta - \left(\frac{n_2}{n_1}\right)^2}}{\sqrt{\left(1+\left(\frac{n_2}{n_1}\right)^2\right)\sin^2\theta\left(\frac{n_2}{n_1}\right)^2}}$$

$$E^\mathrm{r}_{0,2\perp} = \frac{E_{0,2\perp}}{E_{1\perp}} = \frac{2\cdot\cos\theta}{\sqrt{1-\left(\frac{n_2}{n_1}\right)^2}}$$

$$n_2 = F_V\cdot n_{\mathrm{TiO_2}} + (1-F_V)\cdot n_{\mathrm{H_2O}}$$

$$F_V = \frac{V_{\mathrm{TiO_2}}}{V_\mathrm{total}} = \frac{V_{\mathrm{TiO_2}}}{V_{\mathrm{TiO_2}} + V_{\mathrm{H_2O}} + V^\mathrm{add}_{H_2\mathrm{O}}}$$

$E^\mathrm{r}_{0,2\mathrm{II}}$ and $E^\mathrm{r}_{0,2\perp}$ are the relative amplitudes of the electric field (in z = 0, in the medium 2) of the parallel and perpendicular polarized light with respect to the incident plane. $E_{1\mathrm{II}}$ and $E_{1\perp}$ are the amplitudes in the medium 1, where for nonpolarized light $E_{1\perp} = E_{1\mathrm{II}}$. F_V is the TiO_2 volume fraction in the layer of particles. n_2 is calculated as the average of the refraction indexes (in volume) of the TiO_2 and the water in between the particles.

Here we must note that F_V is slightly modified according to the deaggregation of particles by the introduction of $V^\mathrm{add}_{\mathrm{H_2O}}$, which is the additional amount of water entering the layer upon UV irradiation. Under dark conditions, $V^\mathrm{add}_{\mathrm{H_2O}}$ = 0 and determines

Table 1. Measured Absorbance Increments (A) Relative to the First Spectrum under Dark Conditions (Figure 4), ATR Absorption Parameters (eq 5), Additional Water Volume $V^{add}_{H_2O}$ (Figure 6), Penetration Depths (d_p), and TiO_2 Layer Thicknesses (z_2) Spanning 7.9 h of Continuous UVA Illumination[a]

time/min	A at 1643 cm^{-1} [b]	a	$V^{add}_{H_2O}/\mu L$	$d_p/\mu m$	$z_2/\mu m$
2.15					
32.35					
64.72					
97.07	0.0408	0.0104	0.021 ± 0.004	1.577	1.745
129.44	0.0515	0.0131	0.028 ± 0.005	1.556	1.758
161.80	0.0606	0.0154	0.033 ± 0.006	1.537	1.767
194.15	0.0677	0.0172	0.037 ± 0.007	1.527	1.778
224.34	0.0768	0.0194	0.043 ± 0.007	1.509	1.789
256.63	0.0947	0.0239	0.055 ± 0.009	1.477	1.813
288.91	0.1016	0.0257	0.060 ± 0.010	1.464	1.822
321.19	0.1205	0.0304	0.073 ± 0.012	1.432	1.848
353.49	0.1377	0.0346	0.086 ± 0.015	1.404	1.877
385.78	0.1538	0.0386	0.100 ± 0.017	1.379	1.903
418.06	0.1725	0.0432	0.116 ± 0.020	1.350	1.937
446.01	0.1866	0.0466	0.129 ± 0.023	1.329	1.965
467.50	0.2056	0.0512	0.149 ± 0.026	1.300	2.004

[a] Uncertainties of d_p and z_2 values range between 12 and 19% and 15 and 17%, respectively. The results are plotted below to show the tendency they define (Figure 8). [b] Absorbance bands in Figure 4 have been fitted with the following function $y(x) = \kappa \cdot e^{(-(x-\delta)^2/2\cdot\omega^2)}$ optimizing κ, δ, and ω to minimize interferences from incomplete cancellations of water vapor, the absorbance values correspond to the maxima at 1643 cm^{-1}. $n_1 = 2.60737$ at 0.6084 μm (ref 43), $n_{H_2O} = 1.333$ at 25 °C and 0.6084 μm (ref 44), $n_{TiO_2} = 2.488$ at 0.6084 μm (ref 43), $z_1 = 0$ (surface of the ZnSe crystal), $z_2 = 1.7 \pm 0.3$ μm under dark conditions (ref 45), $x \times y = 4.896$ cm^2 (ZnSe crystal surface), and $\varepsilon = 21.65$ $M^{-1}\cdot cm^{-1}$ at 1643.5 cm^{-1} (ref 46). F_V and C_{H_2O}, under dark conditions, are 0.35 and 35.82 M, respectively.

the magnitude of elongation of the layer perpendicularly to the ZnSe crystal's surface: $V^{add}_{H_2O} = x \times y \times (z_{2@t=1} - z_{2@t=2})$. (See Figure 6.)

Finally, because the coefficient of extinction is usually written as the product of the molar extinction coefficient, ε, and the concentration of the absorbing species, C

$$a = \varepsilon \cdot C$$

recalling eqs 3 and 4, the absorption parameter results in the expression

$$a = \varepsilon \cdot C \cdot d_e$$

which allows us to calculate concentrations, C, from measured absorbance values, A.

The spectroscopic absorbance is defined as the inverse logarithm of the transmittance

$$A = -\log\left(\frac{I}{I_0}\right)$$

Using eq 2 for the ATR transmittance for multiple reflections, N, the measurable A takes the form[42]

$$A = -\log(1-a)^N \quad (5)$$

Now, measuring the increment of A referenced to the value under dark conditions, we can calculate the increment of a, and

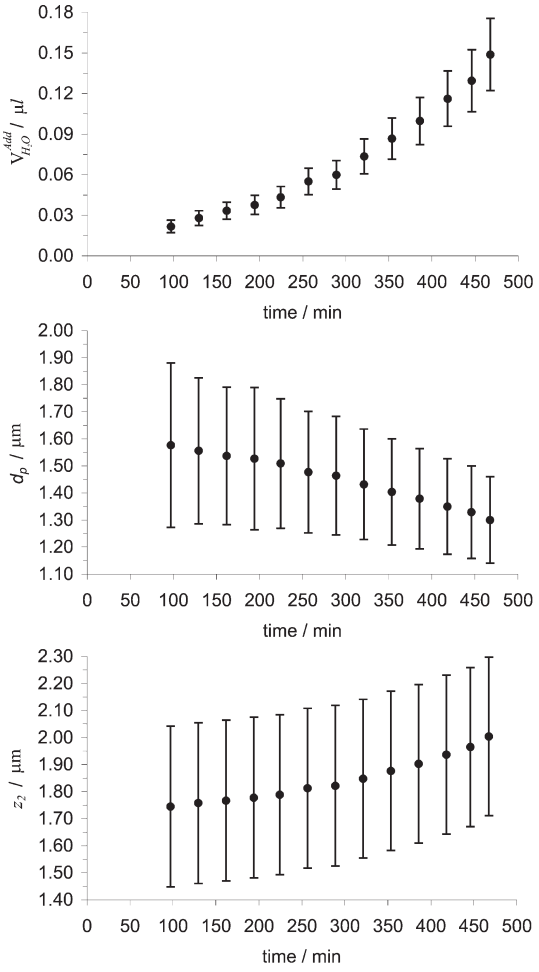

Figure 8. $V^{add}_{H_2O}$, d_p, and z_2 as functions of time.

determine $V^{add}_{H_2O}$ and z_2 because C and d_e can be written as a function of only this variable. Table 1 lists the measured and calculated values.

Figure 8 shows the results obtained for $V^{add}_{H_2O}$, d_p, and z_2. As depicted in the evolution of $V^{add}_{H_2O}$ in time, 0.15 μL of water, which is an increment of 18%, enters the TiO_2 layer whose thickness increases in 0.3 μm after 7.9 h of UVA illumination. If the layer of TiO_2 particles becomes less dense because some agglomerates deaggregate, then one could expect that those particles no longer bonded to their original agglomerate are therefore weakly attached to the layer and may easily diffuse to the bulk solution. However, we have not detected loose particles in our experiments, and the layer appears to maintain its stability after 7.9 h of illumination and continuous circulation of the aqueous phase. Interestingly, the penetration depth of the evanescent wave, d_p, decreases to the order or the thickness of the TiO_2 layer, an extent that should be considered in prolonged photocatalytic measurements aiming to probe the entire section of the layer. It is worthy to note that with an expansion of the layer on top of the ZnSe crystal by incorporation of water, d_p decreases according to the decrease in its refractive, n_2. A smaller d_p corresponds to a lower light intensity because a smaller number of photons will evanesce at that place and will therefore end up with a proportional lower absorption of light. However, an increase in the absorbance at 1643 cm^{-1} is observed (Figure 4), and as Figure 8 (please compare middle and bottom) demonstrates, the evanescent wave remains within the

thickness of the layer over the entire irradiation period, and the calculated volume of water incorporating in the layer, $V^{add}_{H_2O}$, might be subjected to a slight underestimation. We thus confirm that the assumption taken at the start ensures the calculation of such a water volume free of any light absorption enhancement effect.

The large uncertainties in the d_p and z_2 values are due to the original uncertainty in the layer thickness. The z_2 value under dark conditions is set equal to the thickness of the dry layer. We assume that water fills the space between the particles upon contact of the bulk solution without enlarging the thickness of the layer. The expansion occurs, in our model, only under UVA irradiation, when the particles separate from each other, thus allowing an extra amount of water to enter into the layer. We also assume that the deaggregation of particles agglomerates occur uniformly within the entire volume occupied by the layer. (No gradients in the z direction are considered from either the top or the bottom of the layer.) Because the layer is restricted to expand only in the z direction, we assume a convenient rapid rearrangement of the particles to properly distribute in the new increased volume. Finally, we must mention that an important assumption has been also made concerning the volume of water in between the particles. We assumed that the properties of the water molecules in that confined space are the same as those of bulk water, for example, density and structure. Otherwise, the bending mode of water traced in Figure 4 as a function of time may be subjected to further interpretations,[47] beyond the fact that it simply represents an additional volume of liquid water in the optical path of the IR beam, as considered here.

CONCLUSIONS

Alternative aspects of UVA absorption by TiO_2 are evidenced via its consequences. The systems appear to be capable of using the thermal energy freed by recombination of electron−hole pairs and investing it in the deaggregation of some particles agglomerates. If the newly exposed surface area possesses the same properties as the rest of the already exposed surface, then the impact in the photocatalytic process is straightforward. An enlargement of the surface area increases the adsorption capacity and can definitively lead to a higher degradation rate. The incoming liquid volume may also facilitate the transportation of the adsorbant from the solution to the surface.

We remark that the experiments carried out by Pagel et al.[22,27] employed a laser-pulsed UV light source of higher intensity than the one employed in the present work. However, on the basis of the present results, we believe that the deaggregation phenomenon can also proceed in systems under continuous and relatively low UVA irradiation. Regarding energetic considerations, it must be kept in mind that if the released energy upon recombination can be used by the system to separate particles, that is, to break the bonds that maintain them together, other bonds of interest such as those within the adsorbant compounds or on the TiO_2 surface might also be broken by this indirect effect of light mediated by the photocatalyst. A more conclusive proof will be provided by a forthcoming study aimed to check quantitatively the energy requirements in such systems.

APPENDIX: CALCULATION OF UNCERTAINTIES

The structure of eq 1 prevents an algebraic transformation that allows an analytical calculation of $V^{add}_{H_2O}$. Therefore, the calculation of uncertainties via error propagation was impossible. Alternatively, eq 1 was solved numerically, and the uncertainties were estimated by Monte Carlo simulations. $V^{add}_{H_2O}$ was calculated choosing randomly Gaussian distributed numbers for n_1, n_{TiO_2}, n_{H_2O}, V_{TiO_2}, V_{H_2O}, $z_{2\ at\ t=1}$, and a. The uncertainties were set to 1% for all refraction indexes, 5% for the volumes V_{H_2O} and V_{TiO_2}, 10^{-5} cm for the initial thickness of the TiO_2 layer, and 0.0013 for all the a values. For each a value, a large number of $V^{add}_{H_2O}$ values was calculated, for which their mean value and standard deviations were determined, and for every calculated $V^{add}_{H_2O}$ value, d_p and a z_2 values were obtained for which their corresponding mean value and standard deviations were also evaluated. The calculation of 100000 $V^{add}_{H_2O}$ values yielded the satisfying precision, for example, when the standard deviation was one order of magnitude bigger than the third digit of the mean values upon convergence.

AUTHOR INFORMATION

Corresponding Author

*E-mail: cbmendive@mdp.edu.ar. Tel: 0054 223 475 6167

REFERENCES

(1) Fujishima, A.; Honda, K. *Nature* **1972**, *238*, 37–38.
(2) Hoffmann, M. R.; Martin, S. T.; Choi, W.; Bahnemann, D. W. *Chem. Rev.* **1995**, *95*, 69–96.
(3) Fujishima, A.; Zhang, X.; Tryk, D. *Surf. Sci. Rep.* **2008**, *63*, 515–582.
(4) Linsebigler, A. L.; Lu, G.; Yates, J. T. J. *Chem. Rev.* **1995**, *95*, 735–758.
(5) Agrios, A. G.; Pichat, P. *J. Photochem. Photobiol., A* **2006**, *180*, 130–135.
(6) Gaya, U.; Abdullah, A. *J. Photochem. Photobiol., C* **2008**, *9*, 1–12.
(7) Tachikawa, T.; Fujitsuka, M.; Majima, T. *J. Phys. Chem. B* **2007**, *111*, 5259–5275.
(8) Grassian, V. H. *J. Phys. Chem. C* **2008**, *112*, 18303–18313.
(9) Mccullagh, C.; Robertson, J. M. C.; Bahnemann, D. W.; Robertson, P. K. J. *Res. Chem. Intermed.* **2007**, *33*, 359–375.
(10) Diebold, U. *Surf. Sci. Rep.* **2003**, *48*, 53–229.
(11) Palmisano, G.; Augugliaro, V.; Pagliaro, M.; Palmisano, L. *Chem. Commun.* **2007**, 3425–3437.
(12) Hakki, A.; Dillert, R.; Bahnemann, D. *Catal. Today* **2009**, *144*, 154–159.
(13) Ravelli, D.; Dondi, D.; Fagnoni, M.; Albini, A. *Chem. Soc. Rev.* **2009**, *38*, 1999–2011.
(14) Marinković, S.; Hoffmann, N. *Chem. Commun.* **2001**, *78*, 1576–1577.
(15) Zhang, H.; Chen, G.; Bahnemann, D. W. *J. Mater. Chem.* **2009**, *19*, 5089.
(16) Smith, A. M.; Nie, S. *Acc. Chem. Res.* **2010**, *43*, 190–200.
(17) Hu, Y. H.; Wang, H.; Hu, B. *ChemSusChem* **2010**, *3*, 782–796.
(18) Shapovalov, V. I. *Glass Phys. Chem.* **2010**, *36*, 121–157.
(19) Hernández-Alonso, M. D.; Fresno, F.; Suárez, S.; Coronado, J. M. *Energy Environ. Sci.* **2009**, *2*, 1231.
(20) Wang, C.-Y.; Bttcher, C.; Bahnemann, D. W.; Dohrmann, J. K. *J. Mater. Chem.* **2003**, *13*, 2322.
(21) Ismail, A. A.; Bahnemann, D. W.; Robben, L.; Yarovyi, V.; Wark, M. *Chem. Mater.* **2010**, *22*, 108–116.
(22) Wang, C.-Y.; Pagel, R.; Bahnemann, D. W. *J. Phys. Chem. B* **2004**, *108*, 14082–14092.
(23) Sakai, N.; Fujishima, A.; Watanabe, T.; Hashimoto, K. *J. Phys. Chem. B* **2003**, *107*, 1028–1035.
(24) Takeuchi, M.; Sakamoto, K.; Martra, G.; Coluccia, S.; Anpo, M. *J. Phys. Chem. B* **2005**, *109*, 15422–15428.
(25) Zubkov, T.; Stahl, D.; Thompson, T. L.; Panayotov, D.; Diwald, O.; Yates, J. T. *J. Phys. Chem. B* **2005**, *109*, 15454–15462.
(26) Mendive, C. B.; Blesa, M. A.; Bahnemann, D. *Water Sci. Technol.* **2007**, *55*, 139–145.
(27) Pagel, R. Ph.D. Thesis, Frei University: Berlin, Germany, 2004.

(28) Mendive, C. B.; Bredow, T.; Feldhoff, A.; Blesa, M. A.; Bahnemann, D. *Phys. Chem. Chem. Phys.* **2009**, *11*, 1794–1808.
(29) Mendive, C. B.; Bredow, T.; Blesa, M. A.; Bahnemann, D. W. *Phys. Chem. Chem. Phys.* **2006**, *8*, 3232–3247.
(30) Berger, T.; Sterrer, M.; Diwald, O.; Knözinger, E.; Panayotov, D.; Thompson, T. L.; Yates, J. T. *J. Phys. Chem. B* **2005**, *109*, 6061–6068.
(31) Ghosh, H. N.; Asbury, J. B.; Lian, T. *J. Phys. Chem. B* **1998**, *102*, 6482–6486.
(32) Jug, K.; Nair, N.; Bredow, T. *Surf. Sci.* **2005**, *590*, 9–20.
(33) Sun, C. H.; Liu, L. M.; Selloni, A.; Lu, G. Q. M.; Smith, S. C. *J. Mater. Chem.* **2010**, *20*, 10319–10334.
(34) Feldhoff, A.; Mendive, C.; Bredow, T.; Bahnemann, D. *ChemPhysChem* **2007**, *8*, 805–809.
(35) Skoog, D. A.; Holler, F. J.; Nieman, T. A. *Principles of Instrumental Analysis*, 5th edition; McGraw Hill: Madrid, 2001.
(36) Henderson, M. A. *Surf. Sci.* **1996**, *355*, 151–166.
(37) Henderson, M. A. *Surf. Sci. Rep.* **2011**, *66*, 185–297.
(38) Takeuchi, M.; Martra, G.; Coluccia, S.; Anpo, M. *J. Phys. Chem. B* **2005**, *109*, 7387–7391.
(39) Berger, T.; Diwald, O.; Knözinger, E.; Sterrer, M.; Yates, J. T. *Phys. Chem. Chem. Phys.* **2006**, *8*, 1822–1826.
(40) Harrick, N. J. *Appl. Spectrosc. Rev.* **1967**, *21*, 327.
(41) Tompkins, H. G. *Appl. Spectrosc.* **1974**, *28*, 335.
(42) Harrick, N. J. *J. Opt. Soc. Am.* **1965**, *55*, 851.
(43) Bass, M. *Handbook of Optics*; Bass, M., Ed.; McGraw-Hill: New York, 2010; Vol. 1, p 21.5.
(44) Daimon, M.; Masumura, A. *Appl. Opt.* **2007**, *46*, 3811–3820.
(45) Hug, S. J.; Sulzberger, B. *Langmuir* **1994**, *10*, 3587–3597.
(46) Max, J.-J.; Chapados, C. *J. Chem. Phys.* **2009**, *130*, 124513.
(47) Zheng, J.-M.; Chin, W.-C.; Khijniak, E.; Pollack, G. H. *Adv. Colloid Interface Sci.* **2006**, *127*, 19–27.